

Overview of the ATLAS detector at LHC¹

I. Efthymiopoulos *University of Geneva*
(for the ATLAS collaboration)

Abstract

ATLAS is a general-purpose experiment that will exploit the full potential of the LHC p-p collision program. The design aspects of the ATLAS sub-detectors are described here, including performance results from the prototypes being built in the past years. Most of the information is taken from the recently published Technical Design Reports for all of the sub-systems of the experiment. In addition, some highlights of the LHC machine and its challenges are described in the beginning.

1 The LHC Machine

The **Large Hadron Collider (LHC)** is a high-energy, high luminosity proton--proton collider to be built in the existing LEP tunnel at CERN[1]. It will collide proton beams of 7 TeV and its design luminosity is $10^{34} \text{ cm}^{-2}\text{s}^{-1}$. The primary purpose of the LHC is to search for and to study new physics. Although with the LEP results the Standard Model is tested sometimes to better than 1 % level, some fundamental questions are still open. In particular, one hopes to understand the origin of electroweak symmetry breaking (masses of W and Z bosons), looking primarily for one or more Higgs bosons, for example. The LHC can also be used to search for Supersymmetric (SUSY) particles which -if exist- will be produced in some cases with large rates, since the cross-sections for producing for example squarks and gluinos are large. Some other possibilities for new physics that could be studied at LHC are: quark compositeness, leptoquarks, and heavy vector bosons (W', Z'). And last but not least, with the new energy regime that opens, there is always room for the unexpected.

Experiments at LHC will be able to make many measurements related to known physics, such as top decay properties, B-physics and numerous cross-section measurements (W, Z, γ and jet production, for example). The B-physics programme will include studies of CP violation which will allow testing of the Standard Model in which CP violation is parametrised within the CKM matrix. It will also include the measurement of B_s^0 oscillations, the search for rare B decays such as $B_d^0 \rightarrow \mu^+ \mu^- (X)$, and the study of doubly-heavy hadrons such as B_c .

The LHC can also be used to collide beams of heavy ions, e.g. lead ions, with a centre-of-mass energy of about 6 TeV per nucleon, but with lower luminosity ($\sim 10^{27} \text{ cm}^{-2}\text{s}^{-1}$) and interaction rate of $\sim 10^4 \text{ s}^{-1}$, compared to 10^9 s^{-1} for p-p collisions. The heavy-ion programme has as its primary objective the search for the quark--gluon plasma. One will try to investigate different stages in the production of the plasma before the formation of the normal hadronic matter: the initial conditions, the quark--gluon plasma, the phase transition and the hadronic matter. Finally it would be possible to operate simultaneously the LHC and a rebuild LEP machines and produce e-p collisions, but this only if there are strong physics arguments in the future.

1. Presented at the XXVII International Meeting on Fundamental Physics, Sierra Nevada, Granada, Spain, February 1-5 1999.



1.1 The experimental environment at LHC

In the LHC machine, bunches of protons in counter-rotating beams will be made to collide at the “interaction points”. An important parameter of the machine is the 25 ns bunch spacing. The LHC will operate at very high luminosity of $10^{34} \text{ cm}^{-2}\text{s}^{-1}$. The total inelastic, non-diffractive cross-section at LHC energies will be about 100 mb, corresponding to an interaction rate of 10^9 Hz . The task of the LHC experiments is to identify and select the interesting events on top of this background. For example, in the case of the Higgs particle with mass 500 GeV, about 17 K events will be produced per year, compared to a total of 1.7×10^{16} events from the inelastic interactions! In addition, with the bunch-crossing rate of 40 MHz (period of 25 ns), about 23 interactions will happen in each bunch crossing (“pile-up”) resulting in about $\sim 10,000$ tracks in the detector within 100 ns, the typical duration of a pulse in the detectors. All these impose stringent requirements to the design and performance of the LHC detectors: they must be rather fast, in order not to integrate the signals from the pile-up events over many bunch crossings; they must be highly granular in order to minimise the contribution of pile-up in a given detector cell.

The high flux of particles from proton-proton interactions (and to a lesser extent from beam losses) places the detectors and associated electronics in a high-radiation environment. Only radiation resistant detectors and read-out electronics can be used.

2 The ATLAS Detector

Among the four experiments for the LHC, different design philosophies have been adopted depending on which strong point each collaboration chose for the detector, in an effort to optimise them, taking into account the physics goals and the need to keep the cost at a reasonable level. ATLAS uses a large ($\sim 20 \text{ m}$ diameter) air-core toroid system for its muon spectrometer, as shown in Figure 1. The electromagnetic (EM) calorimetry uses the liquid-argon technique. In the barrel, an iron-scintillator hadronic calorimeter is used and in the endcap the hadronic calorimeter is of the liquid-argon type. In front of the barrel EM calorimeter (integrated in the same cryostat) is a superconducting-solenoid coil that provides a 2 T field. The inner-tracking system consists of semiconductor detectors in the innermost part and straw-tubes in the outer part.

The basic design considerations for the ATLAS detector can be summarised as follows: very good EM-calorimetry for e, γ identification and measurement; hermetic jet and E_T^{miss} calorimetry; efficient tracking at high luminosity for lepton measurement, b-quark tagging and enhanced e, γ identification; τ and heavy flavour vertexing and reconstruction capability of some B decays (low luminosity running); low p_T thresholds for the trigger. The detector is expected to be operational in the middle of 2005, when the start-up of the LHC machine is planned.

The ATLAS detector concept was first presented in the Letter of Intent (LoI)[2] and later in the Technical Proposal[3]. Since then, the design has evolved guided by detailed physics performance studies, experience from a rigorous and broad R&D programme, and the necessity to stay within cost-effective technologies. The ATLAS experiment is designed, constructed and operated by a world-wide collaboration of scientists and engineers ($\sim 1,800$ members) from 146 institutions and 33 countries. Spain is contributing with three Institutes and a total of about 4.1 % of the ATLAS members.

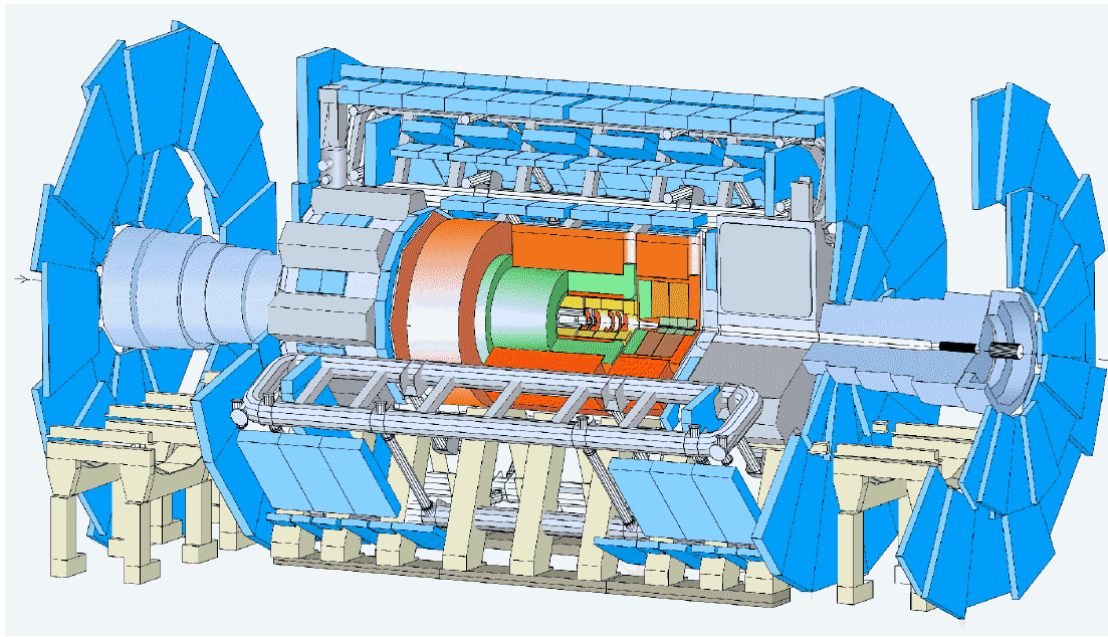


Figure 1 The ATLAS detector.

During 1996 to 1998, the Technical Design Reports for all the major sub-systems of the experiment were written (except for the Computing and the Higher Level Trigger and DAQ systems, which are scheduled for later in order to gain the most from technological developments) and presented to the LHC Committee. Since then, following a positive recommendation by the committee, the collaboration entered in a new phase, that of production, which is now starting for many systems. A set of milestones for the project and a complete scheme for regular progress reviews is defined for each system. Such major progress reviews took place in 1998 for the calorimetry, the muon, the inner detector and the magnet systems, with positive results.

Apart from the various sub-detectors of the experiment which will be described in detail in the following sections, major components are the so called “common projects”, which include the magnet system with its inner tracker solenoid and the outer air core toroids for the muon spectrometer, the three cryostats housing the Liquid Argon Calorimeter, and the supports. Substantial progress has been made in these areas and prototype modules for the coils are under construction along with a large test area [4]. The activity in this area as well as of the overall experimental hall is in the hands of the Technical Coordination of the experiment which has recently published its Technical Design Report.

In the following sections a brief description of the sub-detectors of the experiment is given emphasising the results from their Module-0 program. The status and major milestones for each system are given as well.

2.1 The Inner Detector

The task of the Inner Detector(ID) is to reconstruct the tracks and vertices in the event with high efficiency, contributing, together with the calorimeter and muon systems to the electron, photon and muon measurement and providing the signature for short-lived particle decay vertices. Its acceptance covers the range $|\eta| < 2.5$, matching that of the rest of the ATLAS systems for precision measurements[5].

The detectors used for the ID at LHC have to meet very stringent requirements such as: be very fast, be radiation hard, have high granularity and good momentum resolution. In addition, the amount of material should be kept as small as possible, otherwise the momentum resolution in the tracker itself will be degraded due to the multiple scattering, and the photon and electron identification and energy measurement in the calorimeters will be spoiled. ATLAS has chosen for the innermost part of the tracker semiconductor detectors. A three dimensional cut-away view of the layout of the ID is shown in Figure 2. The outer radius of the tracker cavity is 115 cm and the total length is 7 m. Mechanically, the ID consists of three units: a barrel part extending over 2×80 cm, and two identical end-caps covering the rest of the cylindrical cavity. In the barrel ($|\eta| < 1$), the high-precision detector layers are arranged on concentric cylinders around the beam axis, while the end-cap detectors are mounted on disks perpendicular to the beam axis.

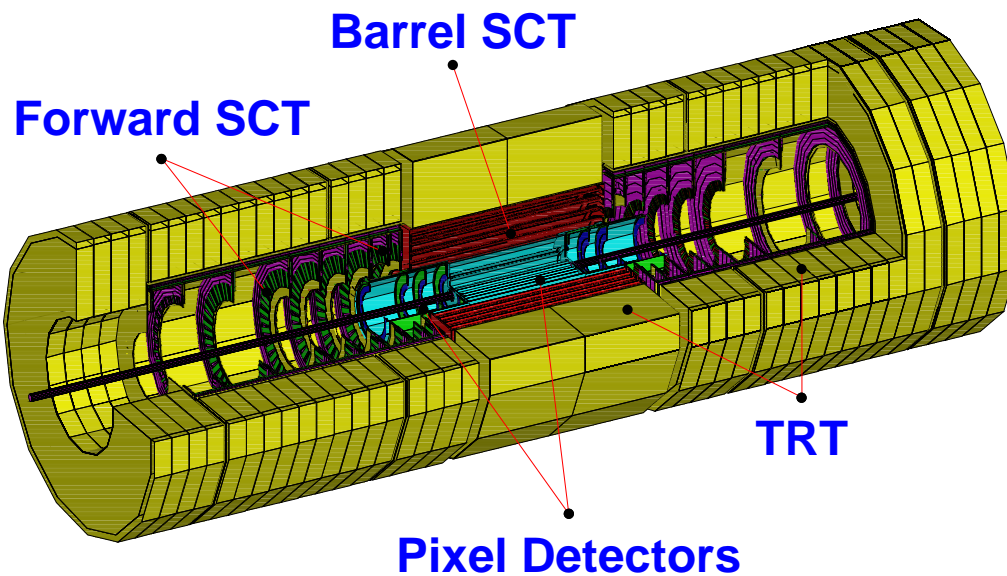


Figure 2 Three dimensional cut-away view of the ATLAS Inner Detector.

Starting from the beam pipe, in the range from 4 to 22 cm in radius, pixel detectors are used which provide up to 3 space points per track. Following that, and up to 56 cm in radius, Si-strip detectors are used, providing four space points per track. For improved momentum reconstruction, pattern recognition and electron identification, a straw tube Transition Radiation Tracker (TRT) is used, which provides 36 points per track (> 7 points/track for e -id). The basic design parameters and resolutions for the space-point measurements are summarised in Table 2-1.

Table 2-1 The main parameters for the Inner Detector. The resolutions quoted are typical values (the actual resolution in each detector depends on $|\eta|$).

Position	Area (m ²)	Resolution $\sigma(\mu\text{m})$	Channels (10 ⁶)	Coverage (η)
Pixel Detector				
1 repl. barrel layer	0.2	$r\phi = 12, z = 66$	16	± 2.5
2 barrel layers	1.4	$r\phi = 12, z = 66$	81	± 1.7
5 ec disks/side	0.7	$r\phi = 12, z = 66$	43	1.7 - 2.5
SCT Detector				
4 barrel layers	34.4	$r\phi = 16, z = 580$	3.2	± 1.4
9 ec wheels/side	26.7	$r\phi = 16, z = 580$	3.0	1.4 - 2.5
TRT Detector				
axial barrel straws		170/straw	0.1	0.7
radial ec straws		170/straw	0.32	0.7 - 2.5

Although the straw hits have lower precision than the ones from the silicon layers, their large number and the fact that they come from larger average radius compensate for that, such that the overall momentum resolution is improved and no single measurement dominates. This means that the overall performance is robust, even in the case that a single system would not perform to its full specification. The full momentum resolution, combining the information from the discrete precision points and the large number of drift-time measurements of the TRT in a global fit through the realistic solenoid field map is shown in Figure 3.

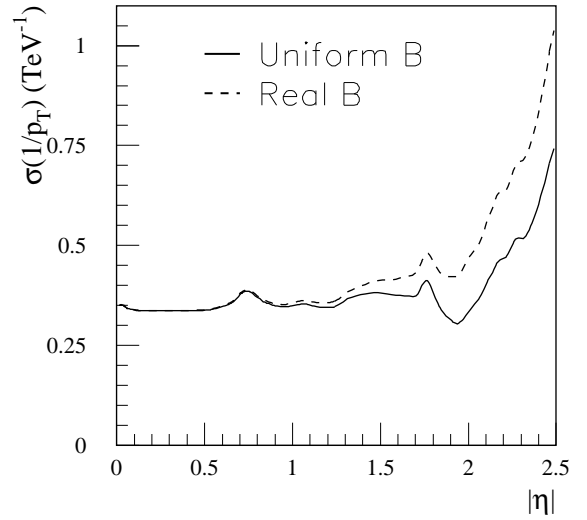


Figure 3 Expected momentum resolution from the ID system.

The innermost silicon layer of the pixel detector located at about 4 cm from the IP, also called “the *B*-layer”, has a substantial contribution to the secondary vertex measurement performance, during the initial low luminosity running of LHC, in particular for the *B* physics sector. Due to the hostile environment at this position in terms of radiation, this layer is designed to be replaceable, during the high luminosity running, since recent physics studies have demonstrated the need for good *b*-tagging performance during all phases of the LHC, in Higgs and supersymmetry searches. The impact parameter resolution shown in Figure 4, can be parametrised in $r\phi$ as $\sigma d_0 = 11 + 60/p_T \sin \vartheta$ and in z as $\sigma(z_0) = 70 + 100/p_T (\sin \vartheta)^3$ (in μm) when the dedicated *B*-physics layer is present.

Every effort has been made to keep the material in the tracking volume to a minimum, by careful design of the active detectors and by the use of low-*Z* materials such as aluminium for the power cables, and carbon-fibre reinforced plastic for the support structures (Figure 5).

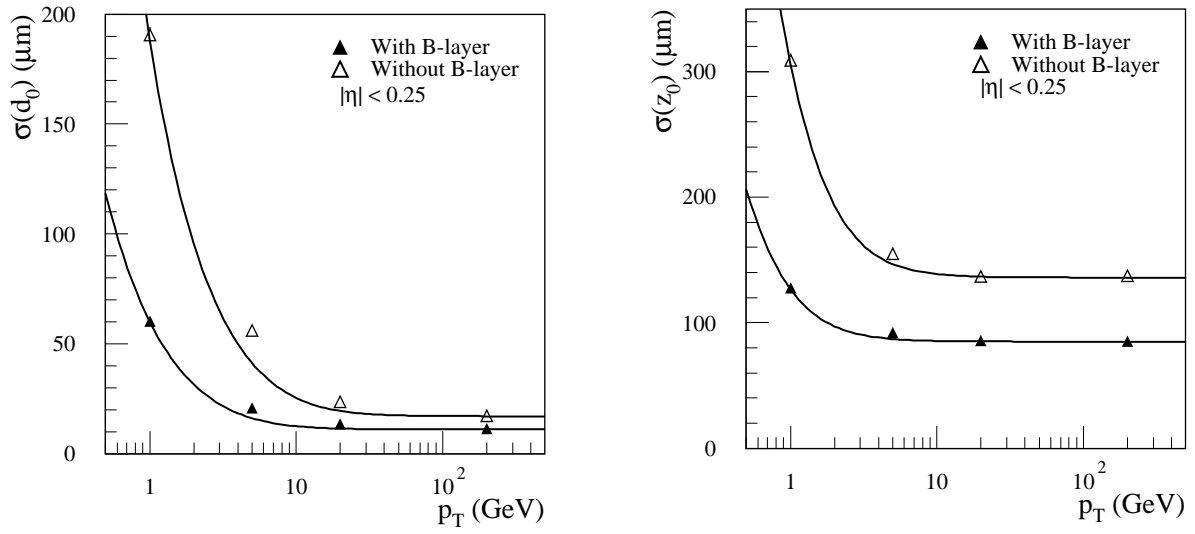


Figure 4 The impact parameter resolution: (left) transverse, (right) longitudinal.



Figure 5 Prototype of the SCT detector support cylinder constructed in Spain.

More details on each sub-system of the ID are presented below.

The ATLAS **Pixel Detector** is composed of modular units. Read out integrated circuits are mounted on a detector substrate to form barrel and disk modules. The detector substrate is silicon, and the current baseline is an n^+n bulk sensor, with a pixel granularity of $50 \mu\text{m} \times 300 \mu\text{m}$. The read out integrated circuits are mounted on the silicon sensor using bonding techniques. An additional integrated circuit for control and clock distribution and data compression is mounted on each module, and flexible cables connect each module to data transmission/control circuitry located within the detector volume. Prototype modules for the detector have been built and tested in the beam (Figure 6). The modules are overlapped on the support structure in order to give hermetic coverage. There are about 1,500 identical barrel modules and about 700 disk modules for the sys-

tem. Both the barrel and disk modules are mounted on special supporting structures and the resulting mechanical structure is very stable and provides the cooling capability to maintain the silicon temperature at $\leq -6^\circ\text{C}$, even with the large heat load from the electronics. Special attention is made to the radiation hardness of the detectors, since they have to withstand over 300 KGy of ionising radiation and over 5×10^{14} neutrons per cm^2 in ten years of operation.

The ATLAS **Semiconductor Tracker (SCT)** system is an order of magnitude larger in surface area than previous generations of silicon microstrip detectors and in addition, it must face radiation levels which will alter the fundamental characteristics of the silicon wafers themselves. The barrel SCT uses four layers of silicon microstrip detectors to provide precision points in the $r\phi$ and z coordinates, using small angle stereo to obtain the z measurement. Each silicon detector is $6.36 \times 6.40 \text{ cm}^2$ with 768 read-out strips each with $80 \mu\text{m}$ pitch. The detector contains 61 m^2 of silicon detectors, with 6.2 million read-out channels. Solutions have been found to the critical issues in the system, and prototype modules have been successfully tested in beams in a magnetic field, showing the required performance in resolution, signal-to-noise and speed. Modules containing both front-end electronics and detectors, irradiated to the level expected for 10 years of LHC operation have been shown to operate within specifications (Figure 7).

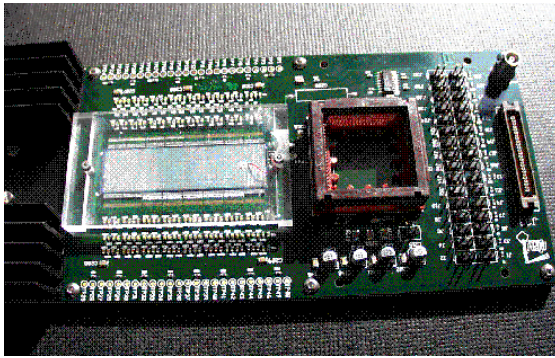


Figure 6 Prototype module for the pixel detector.

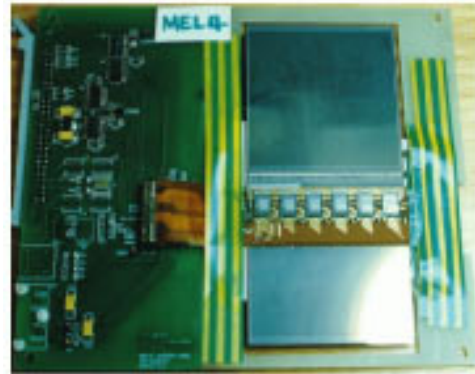


Figure 7 View of an assembled SCT module.

The **Transition Radiation Tracker** is based on the use of straw detectors, which can operate at the very high rates needed, by virtue of their small diameter and the isolation of the sense wires within individual gas envelopes. Electron identification capability is added by employing Xe gas to detect transition-radiation photons created in a radiator between the straws. Each straw is 4 mm in diameter, giving a fast response and good mechanical properties for a maximum straw length of 150 cm. The barrel contains about 50,000 straws, each divided in two at the centre in order to reduce the occupancy and read out at each end. The end-caps contain 320,000 radial straws, with the read-out at the outer radius. The total number of electronic channels is 420,000. Each channel provides a drift-time measurement, giving a spatial resolution of $170 \mu\text{m}$ per straw, and two independent thresholds. These allow the detector to discriminate between tracking hits, which pass the lower threshold, and transition-radiation hits, which pass the higher.

2.2 Calorimetry

The calorimeters will play a crucial role at the LHC. They are required to measure the energy and direction of photons, electrons, isolated hadrons and jets, as well as the missing transverse energy. At the LHC, calorimeters will be the leading detectors for many measurements in physics chan-

nels of prime interest. Combined with the inner tracker, calorimeter measurements are used for electron and photon identification. Fast detector response (< 50 ns) and fine granularity are required to minimise the impact of the pile-up on the physics performance. High radiation resistance is also needed, given the high particle fluxes expected over a period of operation of at least ten years.

ATLAS Calorimetry (Geant)

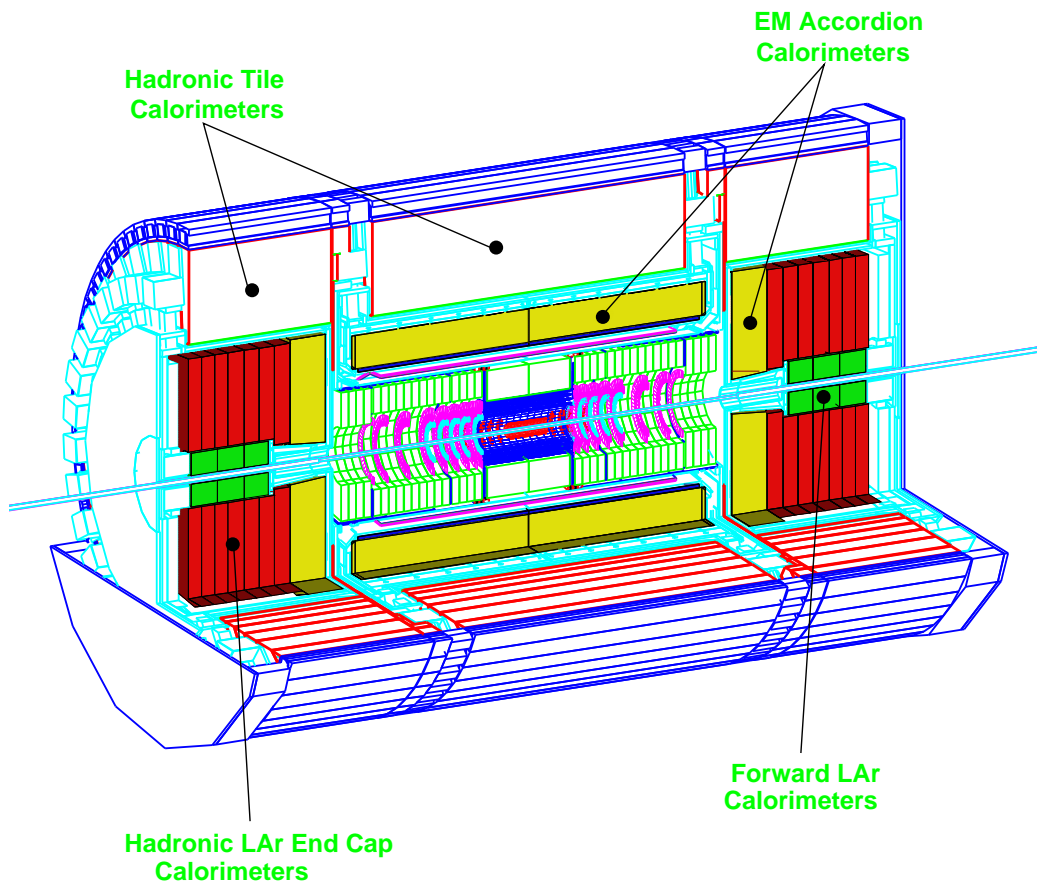


Figure 8 View of the ATLAS calorimetry.

The ATLAS calorimetry covers the range $|\eta| < 5$ using different techniques as best suited to the different requirements and radiation environment. A view of the ATLAS calorimetry is shown in Figure 8. The rapidity coverage and basic granularity of the calorimeters is summarised in Table 2-2. The *EM* calorimeter system is contained in a cylinder of outer radius 2.25 m and a total length of 6.65 m along the beam axis. The barrel hadronic calorimeter system has an outer radius of 4.23 m and a total length of ~ 12 m. The total weight of the calorimeter system is about 4,000 T. The End-Cap *EM*, Hadronic and Forward calorimeters are housed in the same cryostat.

System	η coverage	Granularity ($\Delta\eta\times\Delta\phi$)
EM barrel	$ \eta < 1.475$	0.03×0.1 (s1) 0.025×0.025 (s2) 0.05×0.025 (s3)
Presampler	$ \eta < 1.8$	0.025×0.1
Hadronic barrel	$ \eta < 1.8$	0.1×0.1
Hadronic ec	$1.5 < \eta < 2.5$ $2.5 < \eta < 3.2$	0.1×0.1 0.2×0.2
FWD Calo	$3.2 < \eta < 4.9$	$\sim 0.2 \times 0.2$

3D schematic diagram of the experimental setup for the first experiment. The diagram illustrates the geometry of the detector components and their dimensions.

- Top Surface:** Towers in Sampling 3, $\Delta\phi \times \Delta\eta = 0.0245 \times 0.05$.
- Front Face:** Strip towers in Sampling 1, $\Delta\phi = 0.0245$, $\Delta\eta = 0.0031$.
- Right Face:** Square towers in Sampling 2, $\Delta\phi = 0.0245$.
- Back Face:** Trigger Tower, $\Delta\eta \approx 0.1$, $\Delta\phi = 0.0982$.
- Dimensions:**
 - Height: 1500 mm
 - Width: 470 mm
 - Depth: 37.5 mm / 8 = 4.69 mm
 - Length: 36.8 mm × 4 = 147.3 mm
 - Section widths: 1.7X₀, 4.3X₀, 2X₀, 16X₀
- Coordinate System:** ϕ (polar angle) and η (pseudorapidity).

During 1998 full size detector modules were constructed and put in the beam (Figure 10). The energy resolution for electrons is in agreement with the values obtained from the prototype program, with a sampling term of (9.90-10.4) %, a local constant term of (0.27-0.35) % and a noise term of (280-520) MeV over the full η range. The target figure for the overall constant term (which dominates at high energies, therefore very important for LHC) is 0.7 % which puts stringent requirements on the detector construction, the dead material in front and the calibration precision.

9

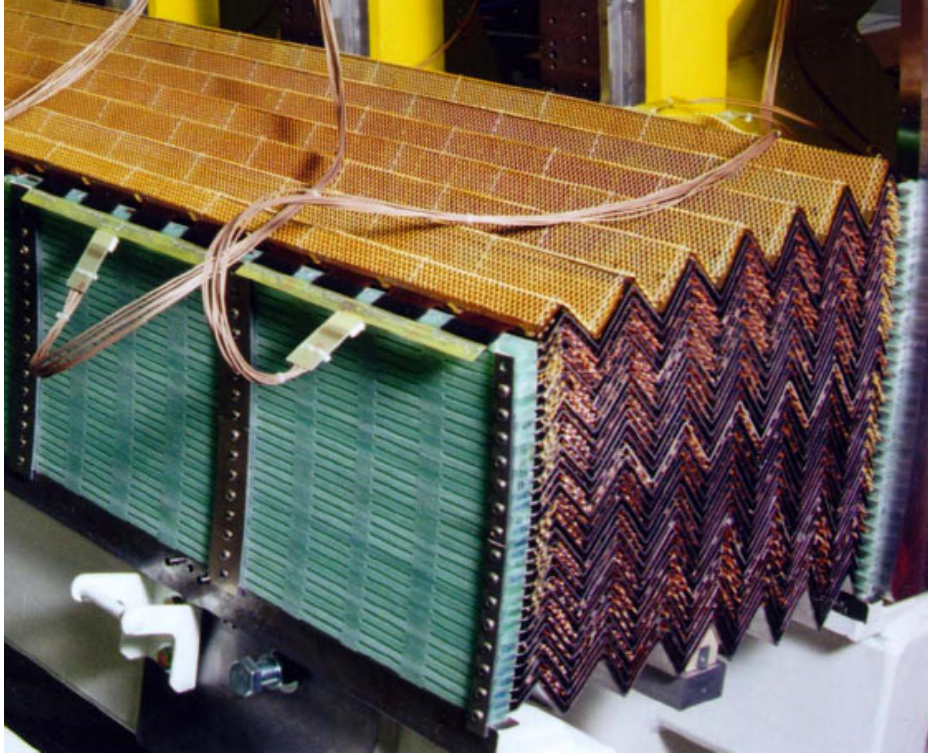


Figure 10 EM barrel calorimeter full size module.

The **Tile Hadronic Calorimeter** covers the range $|\eta| < 1.6$ and it consists of the barrel and the two extended barrel cylinders [8]. The hadronic barrel calorimeter is a cylinder with an inner radius of 2.28 m and an outer radius of 4.23 m. It is divided in three sections: the central barrel and two extended barrels. It is based on a sampling technique with plastic scintillator plates (tiles) embedded in an iron absorber matrix and read out by wave length shifting fibres. The tiles are placed in plane perpendicular to the beam axis and staggered in depth, simplifying the mechanical construction and the fibre routing. In Figure 11 a full size extended barrel calorimeter module is shown.

The calorimeter is segmented in three layers, approximately 1.4 , 4.0 and $1.8 \lambda_{\text{abs}}$ thick at $\eta=0$. Azimuthally, the barrel and extended barrels are divided into 64 modules. In η , the read-out cells, built by grouping fibres to a photomultiplier, are pseudo-projective to the interaction region. The total number of channels is of the order of 10,000. The calorimeter is placed behind the EM calorimeter ($\sim 1.2 \lambda_{\text{abs}}$) and the solenoid coil, resulting in a total active calorimeter thickness (EM+Tile) of $9.2 \lambda_{\text{abs}}$ at $\eta=0$ and a total amount of material in front of the muon system, including the support structure of the Tile calorimeter, of $11 \lambda_{\text{abs}}$ at $\eta=0$.

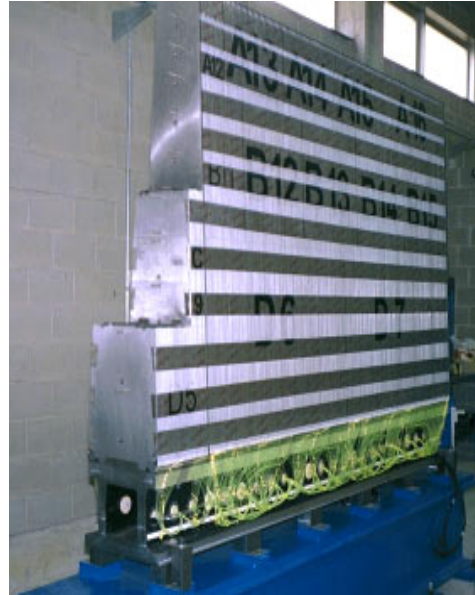


Figure 11 A Tile Calorimeter extended barrel module constructed in Spain.

The required energy resolution is driven by jets measurement, *i.e.* $\Delta(E)/E = 50\%/\sqrt{E} \oplus 3\%$, within $|\eta| < 3$. From the test beam runs with the EM and hadronic prototype modules the pion resolution obtained is $\Delta(E)/E = (38.3 \pm 4.6)\%/\sqrt{E} + (1.62 \pm 0.29)\% \oplus (3.06 \pm 0.18)/E$, well within the specifications for ATLAS.

In the range $1.5 < |\eta| < 4.9$ the **Liquid Argon Hadronic Calorimeter** takes over: the end-cap hadronic calorimeter extends to $|\eta| = 3.2$ while the range $3.1 < |\eta| < 4.9$ is covered by the high-density forward calorimeter. Both the hadronic end-cap and the forward calorimeters are integrated in the same cryostat housing also the EM end-caps. Each hadronic end-cap calorimeter consists of two, equal diameter, independent wheels. The first wheel is built out of 25 mm copper plates, while the second one uses 50 mm plates; in both wheels the gap between consecutive copper plates is 8.5 mm, and is equipped with 3 electrodes that split it in 4 drift spaces of ~ 1.8 mm each. The wheels are divided in two longitudinal read-out segments. The read-out cells are fully pointing in ϕ but only “pseudo pointing” in η . The thickness of the active part of the end-cap calorimeter is $\sim 12 \lambda_{\text{abs}}$.

In ATLAS the **Forward Calorimeter** is integrated in the end-cap cryostat, with the front face at about 5 meters from the interaction point. This makes the forward calorimeter a particularly challenging detector due to the high level of radiation. However, a clear benefit in terms of continuity of coverage, reducing to the minimum the effects of the crack in the transition region around $|\eta| = 3.1$, with advantages to the efficiency of forward jet tagging and the reduction of the tails in the $E_{\text{T}}^{\text{miss}}$ distribution. The forward calorimeter has to accommodate at least $9 \lambda_{\text{abs}}$ of active detector in a rather short longitudinal space. Thus it is a high density detector, consisting of three longitudinal sections, the first one made of copper, and the other two of tungsten. Each of them consists of a metal matrix with regularly spaced longitudinal channels filled with rods. The sensitive medium is Liquid Argon and fills the gap between the rod and matrix. The gaps are 250 microns wide in the first section and 375 (500) microns in the second (last) one. In the forward calorimeter the electronic noise in a jet cone of $\Delta R = 0.5$ is ~ 1 GeV E_{T} at $\eta = 3.2$ and drops quickly to 0.1 GeV in E_{T} at $\eta = 4.6$. The expected jet resolution in the full rapidity range combining the information from the various calorimeters is shown in Figure 12 and is adequate for the measurements to be performed.

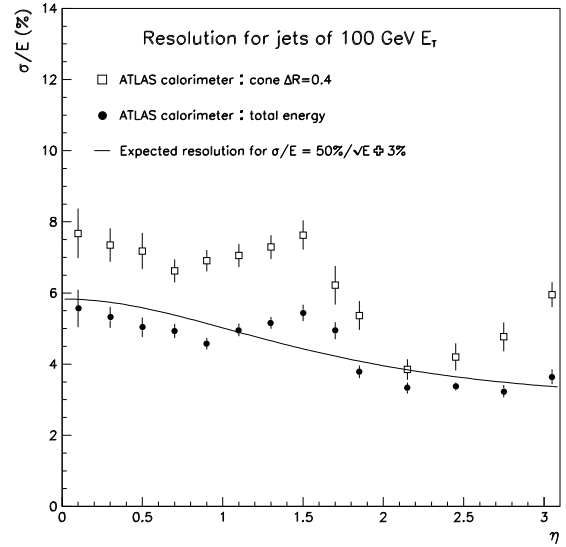


Figure 12 The expected jet resolution in ATLAS for the full rapidity range.

2.3 The Muon Spectrometer

High-momentum final-state muons are among the most promising and robust signatures of physics at the Large Hadron Collider (LHC). The discovery potential of the spectrometer has been optimised on the basis of selected benchmark processes, in particular Standard Model and supersymmetric Higgs decays and new vector bosons. The performance of the apparatus for low transverse momenta which is of interest for beauty physics and CP violation has also been stud-

ied. Important parameters that need to be optimised for maximum physics reach are: resolution, second-coordinate measurement, rapidity coverage of track reconstruction, trigger selectivity, trigger coverage and bunch-crossing identification. To exploit this potential, the ATLAS collaboration has designed a high-resolution muon spectrometer with stand-alone triggering and momentum measurement capability over a wide range of transverse momentum, pseudorapidity, and azimuthal angle [9]. The view of the muon spectrometer is shown in Figure 13.

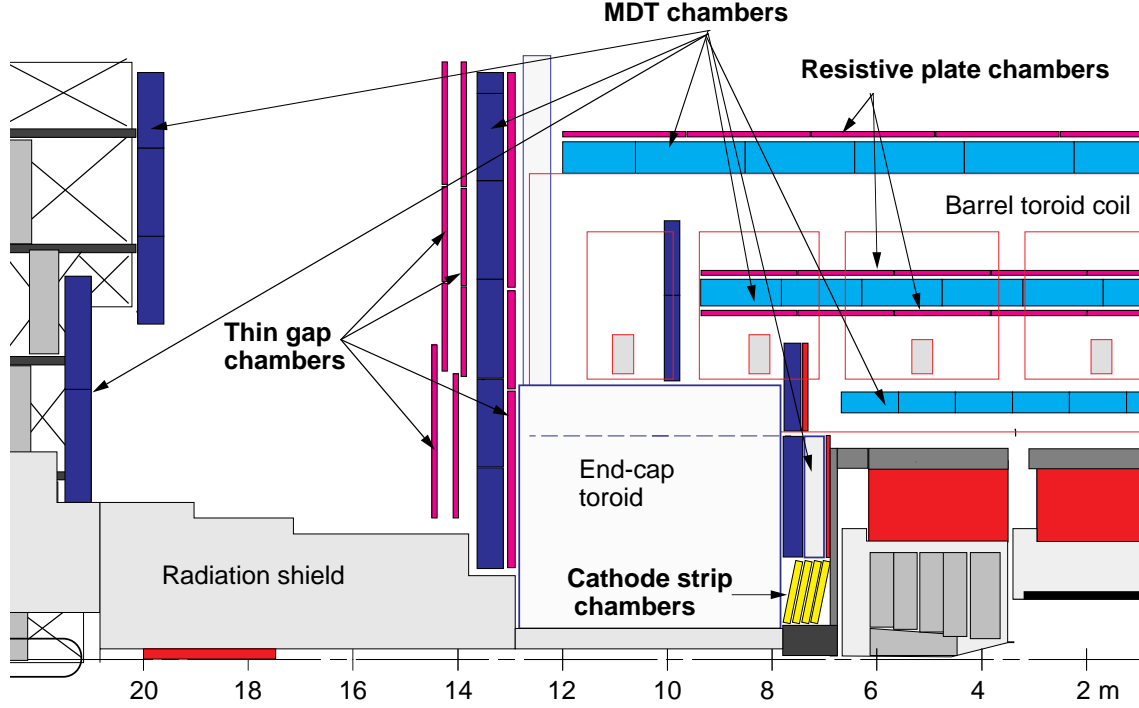


Figure 13 View of the ATLAS muon spectrometer.

The muon spectrometer exploits the magnetic deflection of muon tracks in a system of three large superconducting air-core toroid magnets (one barrel and two end-caps) instrumented with separate-function trigger and high-precision tracking chambers. In the pseudorapidity range $|\eta| < 1$, magnetic bending is provided by a large barrel magnet consisting of eight coils surrounding the hadron calorimeter. For $\sim 1.4 < |\eta| < 2.7$, muon tracks are bent in two smaller end-cap magnets inserted into both ends of the barrel toroid. In the interval $1.0 < |\eta| < 1.4$, referred to as transition region, magnetic deflection is provided by a combination of barrel and end-cap fields. This magnet configuration provides a field that is mostly orthogonal to the muon trajectories, and minimizing the degradation of resolution due to multiple scattering.

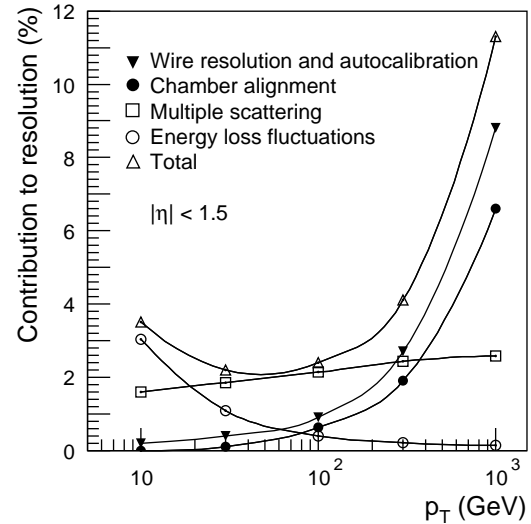


Figure 14 Contributions to the momentum resolution of the muon spectrometer, averaged over $|\eta| < 1$ and azimuthal angle, in a standard sector.

The different contributions to the barrel momentum resolution are shown in Figure 14. The behaviour observed is typical for an open-geometry magnetic spectrometer. The resolution is limited by energy loss fluctuations at small momenta and by detector resolution at high momenta, whereas the multiple scattering effect is approximately momentum-independent. The momentum resolution is typically 2-3 % over most of the kinematic range apart from very high momenta, where it increases to ~ 10 % at $p_T = 1$ TeV. Its dependence in $|\eta|$ is also shown in Figure 15 for $p_T = 100$ GeV muons. The resolution is largely constant over the η range of the spectrometer, with the exception of some spikes at pseudorapidities obstructed by barrel magnet elements, and of an degradation around $\eta = 1.5$ owing to a less bending power in the transition region between barrel and end-cap magnets.

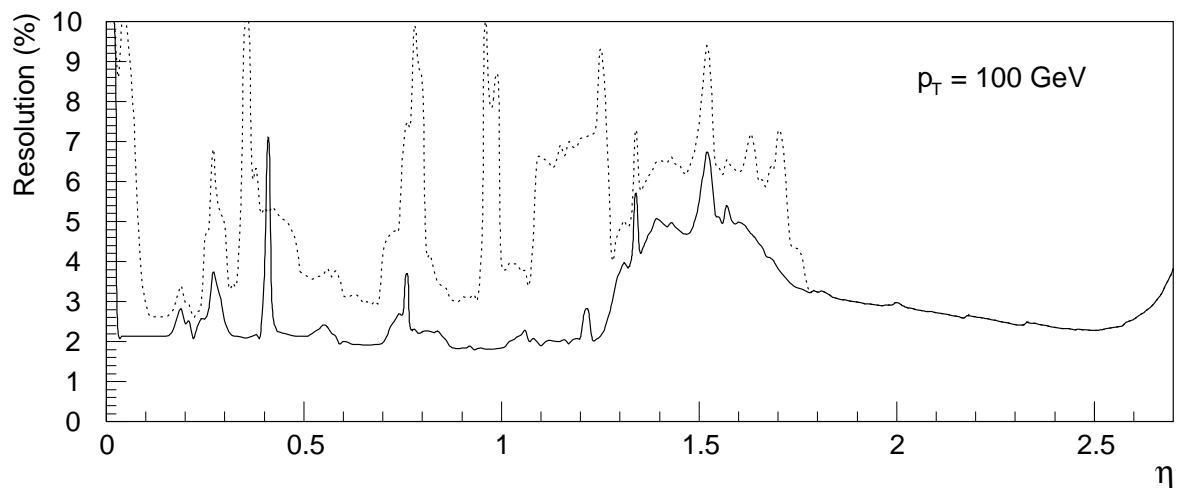


Figure 15 Momentum resolution for $p_T = 100$ GeV as a function of η averaged over all azimuth angles. The solid curve applies to a standard sector; the dotted curve corresponds to one of the bottom sectors, where barrel toroid coils are captured inside the support structure for the inner parts of the detector.

Over most of the pseudorapidity range, a precision measurement of the track coordinates in the principal bending direction of the magnetic field is provided by **Monitored Drift Tubes (MDT)**. The basic detection elements are aluminium tubes of 30 mm diameter and 400 μm wall thickness, with a 50 μm diameter central W-Re wire. The tubes are operated with a non-flammable ArCO_2 mixture at 3 bar absolute pressure. The envisaged working point provides for a non-linear space-time relation with a maximum drift time of ~ 700 ns, a small Lorentz angle, and good ageing properties due to small gas amplification. The single-wire resolution is typically 80 μm . To improve the resolution of a chamber beyond the single-wire limit and to achieve adequate redundancy for pattern recognition, the MDT chambers are constructed from 2×4 monolayers of drift tubes for the inner and 2×3 monolayers for the middle and outer stations. The tubes are arranged in multilayers of three or four monolayers, respectively, on either side of a rigid support structure. The construction of prototypes has demonstrated that they can be built to the required mechanical accuracy of ~ 30 μm . Full size prototype modules have been built and tested in the beam, showing good performance within the specifications for ATLAS.

Cathode Strip Chambers (CSC) are used in the first station of the end-cap region and for pseudorapidities $|\eta| > 2$ to provide a finer granularity which is required to cope with the demanding rate and background conditions. The CSCs are multiwire proportional chambers with cathode strip read-out and with a symmetric cell in which the anode-cathode spacing is equal to the anode wire pitch. The precision coordinate is obtained by measuring the charge induced on the segmented

cathode by the avalanche formed on the anode wire. The anode wire pitch is 2.54 mm and the cathode read-out pitch is 5.08 mm; r.m.s. resolutions of better than 60 μm have been measured in several prototypes. Other important characteristics are small electron drift times (30 ns), good time resolution (7 ns), good two-track resolution, and low neutron sensitivity. The CSCs are arranged in 2×4 layers. The design utilizes low-mass construction materials to minimize multiple scattering and detector weight (Figure 16).

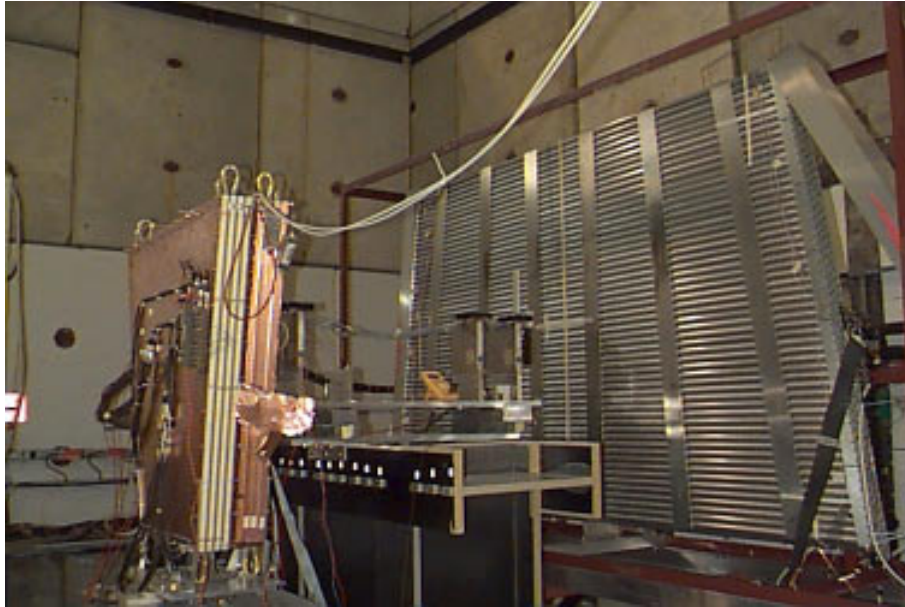


Figure 16 View of the CSC and MDT prototype modules in the test beam setup.

The **Trigger Chambers** for the ATLAS muon spectrometer serve a threefold purpose: bunch crossing identification, requiring a time resolution better than the LHC bunch spacing of 25 ns; a trigger with well-defined p_T cut-off in moderate magnetic fields, requiring a granularity of the order of 1 cm; measurement of the second coordinate in a direction orthogonal to the one measured in the precision chambers with a typical resolution of 5-10 mm.

The proposed system employs two different types of detectors, **Resistive Plate Chambers (RPC)** in the barrel ($|\eta| < 1.4$) and **Thin Gap Chambers (TGC)** in the end-cap region. The trigger chambers cover a total area of about 3650 m^2 in the barrel and 2900 m^2 in the end-cap region, each chamber containing at least two detector layers. The total number of channels is about 350,000 for the barrel and 440,000 in the end-caps.

The RPC is a gaseous detector providing a typical space-time resolution of 1 cm \times 1 ns with digital read-out. The basic RPC unit is a narrow gas gap formed by two parallel resistive bakelite plates, separated by insulating spacers. The TGC chambers are designed in a way similar to multiwire proportional chambers, with the difference that the anode wire pitch is larger than the cathode-anode distance. Signals from the anode wires, arranged parallel to the MDT wires, provide the trigger information together with read-out strips arranged orthogonal to the wires. The read-out strips also serve to measure the second coordinate.

2.4 Trigger/DAQ and Physics Performance

The high interaction rate of LHC puts stringent requirements to the trigger and data-acquisition systems. Only a tiny fraction of the interactions can be recorded for off-line analysis, requiring a trigger selectivity of about one interaction in 10^7 . Furthermore, massive amounts of data have to be transmitted to and stored in buffer memories while the trigger system performs its calculations. Note that, since it is impossible to make a trigger decision within the 25 ns between bunch crossings, the so-called “pipelined readout” has to be used, typically with electronics mounted on the detector. The scheme of the pipelined readout along with the general architecture of the Trigger and DAQ system is illustrated in Figure 17.

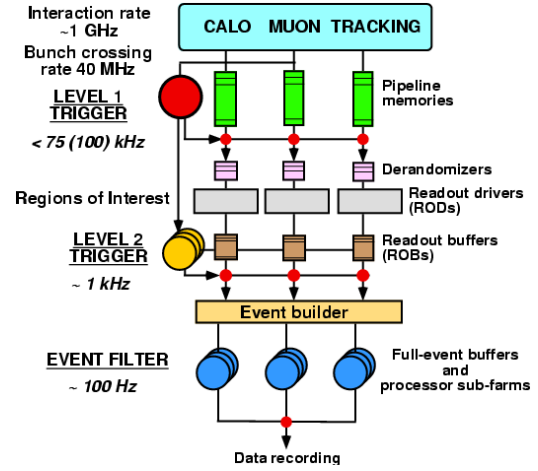


Figure 17 View of the pipelined readout architecture of the ATLAS LHC detector.

After having described all the components of the ATLAS detector, the proof that they perform as a whole can only be demonstrated by the expected results for some interesting physics issues at LHC. One of those is the search for the Higgs, which implies stringent requirements on all detector parts in order to cover a broad mass spectrum with discovery capability in the relevant decay channels. Figure 18 shows that this is achievable over the whole mass range. Another case is the search for Supersymmetry, where it seems clear that -if it exists- it can be discovered through the decay chains of squarks and gluinos to LSP. The real issue will be to extract measurements for well-chosen points in the SUGRA parameter space. If characteristic deviations from the SM appear and they point to some class of models indicating the rough mass scale, then typical kinematic features of the events (such as a sharp cut in the dilepton mass as shown in Figure 19) could further help exploiting constraint fits to a large number of hypotheses.

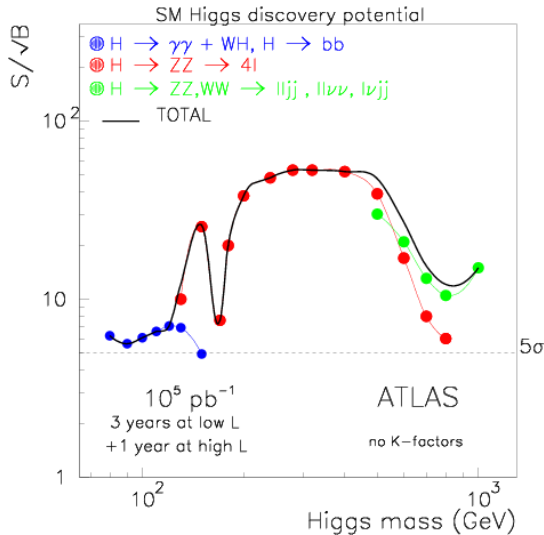


Figure 18 Higgs particle discovery potential for ATLAS.

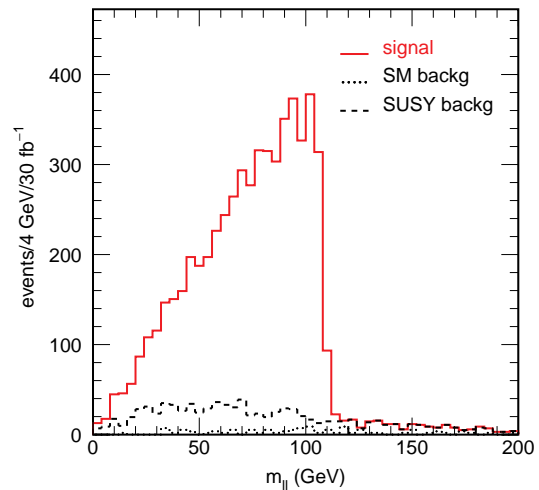


Figure 19 Dilepton signal for SUGRA point 5 (solid), background from other SUSY sources (dashed) and sum of SM backgrounds (dotted).

Concerning the B-physics studies, a rich field for the initial low luminosity, it has been shown that the angles of the unitarity triangle can be measured through asymmetries in the relevant B-decays. With the achievable precision in $\sin 2\beta$ and $\sin 2\alpha$ of ± 0.01 and ± 0.05 respectively, it will be possible to establish direct CP violation. Last, but not least, various Standard Model measurements can be performed. As an example, the error on the W and the top mass which are expected to be 0.02 GeV and 2 GeV in ATLAS respectively put significant constraints on the Higgs mass.

Acknowledgments

I would like to thank the organizers of the XXVII Winter Meeting on Fundamental Physics and in particular Prof. F. del Aguila for the invitation and the hospitality I was treated. Finally I would like to thank all my colleagues who provided material for this presentation and helped me in writing these proceedings.

References

- 1 The Large Hadron Collider, CERN/AC/95--05.
- 2 ATLAS Letter of Intent for a General-Purpose pp Experiment at the Large Hadron Collider at CERN, CERN/LHCC/92--4, LHCC/I2 (1992).
- 3 The ATLAS Technical Proposal for a General Purpose pp Experiment at the Large Hadron Collider at CERN, CERN/LHCC/94-43 (1994).
- 4 ATLAS Magnet System Technical Design Report, CERN/LHCC 97-18, 97-19, 97-20 (1997).
- 5 ATLAS Inner Detector Technical Design Report, CERN/LHCC 97-16, 97-17 (1997).
- 6 ATLAS Liquid Argon Calorimeter Technical Design Report, CERN/LHCC 96-41 (1996).
- 7 ATLAS Calorimeter Performance Technical Design Report, CERN/LHCC/96-40 (1996).
- 8 ATLAS Tile Calorimeter Technical Design Report, CERN/LHCC 96-42 (1996).
- 9 ATLAS Muon Spectrometer Technical Design Report, CERN/LHCC 97-22 (1997).